Vacuum Ultraviolet Spectroscopy of the Carbon Molecule C_3 in Matrix Isolated State: Experiment and Theory

G. Monninger,[†] M. Förderer,[†] P. Gürtler,[‡] S. Kalhofer,[†] S. Petersen,[‡] L. Nemes,[§] P. G. Szalay,[||] and W. Krätschmer*,[†]

Max-Planck-Institut für Kernphysik, Postfach 103980, D-69029 Heidelberg, Germany, Hasylab at Desy, Notkestrasse 85, D-22603 Hamburg, Germany, Chemical Research Center, Research Laboratory for Materials and Environmental Chemistry, Hungarian Academy of Sciences, Pusztaszeri út 59-67, H-1025 Budapest, Hungary, and Department of Theoretical Chemistry, Eötvös Loránd University, P. O. Box 32, H-1518 Budapest, Hungary

Received: November 19, 2001; In Final Form: March 19, 2002

Carbon molecules were produced by evaporation of graphite and matrix-isolated in solid neon and argon. Using synchrotron radiation, the absorption spectra of the carbon clusters were recorded from 1100 to 5600 Å, and the fluorescence or phosphorescence spectra were recorded from 1200 to 9000 Å. We observed an intense, broad absorption band system centered at around 1600 Å in neon and 1700 Å in argon. By measuring the excitation spectrum of the a $^3\Pi_u \rightarrow X\ ^1\Sigma^+_g$ phosphorescence and checking the intensity correlation with the known $^1\Pi_u \leftarrow X\ ^1\Sigma^+_g$ absorption band, we could show that the observed VUV band system is the allowed $^1\Sigma^+_u \leftarrow X\ ^1\Sigma^+_g$ electronic transition of the C_3 molecule. At the blue and the red side of the band system, distinct progressions can be observed which most likely correspond to a symmetric stretch of about $\nu_1 \approx 1100\ cm^{-1}$ and a bending mode of about $\nu_3 \approx 550\ cm^{-1}$, respectively. In the band center, however, a complicated superposition of several vibrational progressions appears indicating that besides the $^1\Sigma^+_u$ state also other states seem to contribute to the absorption. Quantum chemical MR-AQCC calculations suggest that these contributing states are $^1\Pi_g$ states which are close in energy to the $^1\Sigma^+_u$ state and can interact via vibronic coupling, a conjecture supported by preliminary calculations of synthetic spectra in which such coupling was included. Furthermore, the calculations show that the $^1\Sigma^+_u$ energy decreases upon bending, leading to a complex landscape of energy surfaces which include avoided crossing type features, and rendering more detailed spectral calculations difficult.

1. Introduction

Since the first observation of the 4050 Å band system in the spectra of comets in 1881[1] and the identification of the carrier molecule C_3 seventy years later,[2] carbon clusters gained growing experimental and theoretical interest. Reviews on smaller carbon species were given by Weltner and van Zee[3] and, for the more recent developments, by van Orten and Saykally.[4] During the past decades, the role of carbon molecules in astrophysics and combustion chemistry was recognized to an increasing degree,[5,6] and recently, fullerenes, i.e., large, closed cage carbon molecules, gained considerable attention.[7,8]

The carbon cluster C_3 is the dominant constituent of carbon vapor generated by heating graphite to about 3000 K. Under these conditions, the vapor consists approximately of atomic C (10%), C_2 (20%), C_3 (70%), and a rather small fraction of larger species (<1%).[9−11] Many groups investigated the spectra of C_3 by the matrix-isolation technique, in which carbon molecules are trapped along with an excess of an inert gas (e.g., argon or neon) on a cold (5−15 K) substrate (see, e.g., ref 3, 4, and 12−16). The advantages of this technique are that no molecular rotations occur in the matrix and that, because of the low temperature, the transitions emerge exclusively from the electronic and vibrational ground state. This simplifies the absorption spectra; however, the interaction of the molecules with the matrix introduces some artifacts; that is, it shifts and broadens the absorptions.

The ground-state configuration of C_3 exhibits completely filled orbitals $...(1\pi_u)^4(3\sigma_u)^2(1\pi_g)^0$. The most prominent absorption in the near UV is the "cometary" band at 4050 Å assigned to a $^1\Pi_u \leftarrow X\ ^1\Sigma^+_g$ transition in which an electron in the $3\sigma_u$ orbital is promoted into the empty $1\pi_g$ orbital. Because of matrix interactions, the "cometary" absorption is shifted toward 4070 Å in solid neon and 4100 Å in solid argon. In emission, a strong C_3 phosphorescence at about 5900 Å was observed and tentatively assigned by Weltner and co-workers to the lowest triplet transition a $^3\Pi_u \leftarrow X\ ^1\Sigma^+_g$[13]. The assignment was later confirmed by Bondybey and English[15] and supported by quantum chemical calculations (see, e.g., ref 17). A recent work on the C_3 phosphorescence can be found in ref 18.

Besides the transition leading to the 4050 Å band, one expects an allowed, i.e., rather strong, $^1\Sigma^+_u \leftarrow {}^1\Sigma^+_g$ absorption system of C_3 to occur at considerably shorter wavelength. This band, already predicted by Pitzer and Clementi[19] in their classical article of 1959, should originate from the promotion of a $1\pi_u$ electron into the empty $1\pi_g$ orbital. Early quantum chemical calculations were carried out by Williams[20] and Römelt et al.[21] The later authors used the MRD CI method to calculate the excitation energy of the $^1\Sigma^+_u$ state to be about 8 eV. Experi-

* To whom correspondence should be addressed. E-mail: kraetschmer@mpi-hd.mpg.de.
[†] Max-Planck-Institut für Kernphysik.
[‡] Hasylab at Desy.
[§] Hungarian Academy of Sciences.
[||] Eötvös Loránd University.

10.1021/jp0142536 CCC: $22.00
Published on Web 05/25/2002

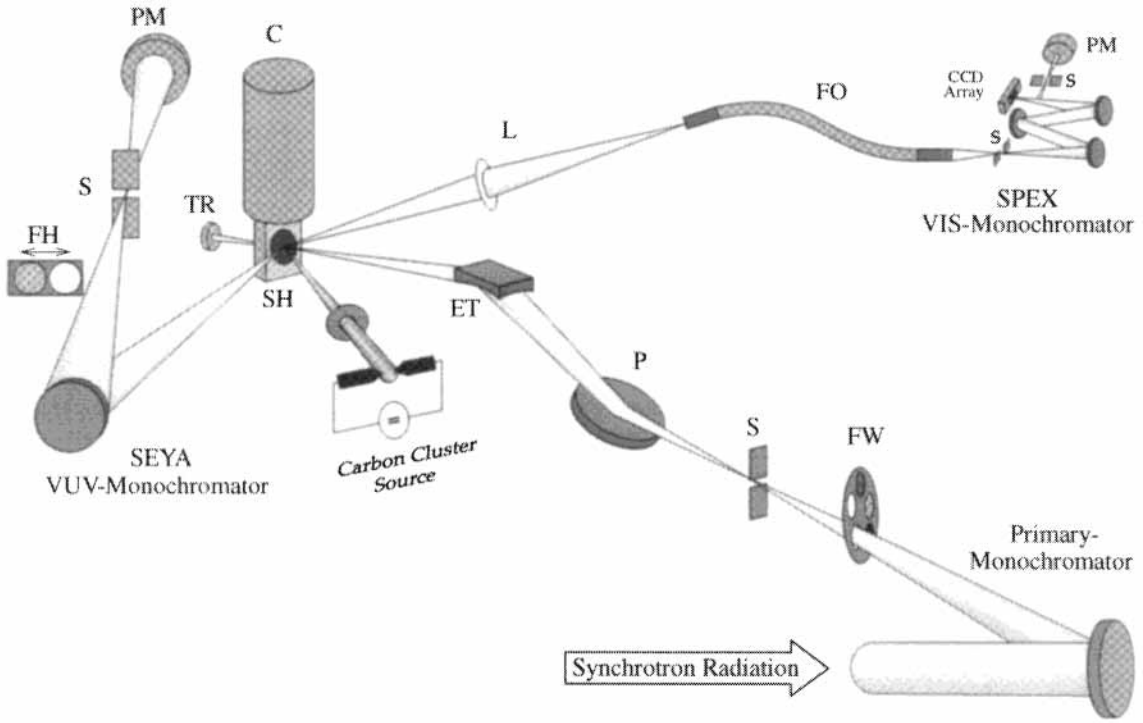

Figure 1. Experimental setup of the station HIGITI at Hasylab. Abbreviations: filter wheel (FW), slit (S), planar mirror (P), Torroid ellipsoidal mirror (ET), sample holder with MgF_2 substrate (SH), liquid helium cryostat (C), lens (L), fiber optic (FO), photomultiplier (PM), filter holder of the Seya monochromator (FH). When the synchrotron radiation beam is elongated through the MgF_2 substrate, the transmission spectra are recorded behind the sample holder (SH) with a photomultiplier (TR). For further details, see text.

mental evidence for this band was provided for the first time in 1982 by Chang and Graham who isolated carbon vapor in an argon matrix at 8 K and assigned a spectral feature near 1890 Å (6.6 eV) to this transition.[22] The assignment was supported by intensity correlations with the known $^1\Pi_u \leftarrow X\ ^1\Sigma^+_g$ absorption band system and from spectra obtained by ^{13}C substituted species. However, the band position appears to be in conflict with more recent theoretical predictions, which locate the transition between 7.15 and 8.14 eV.[23,24] The MRD CI calculations of ref 21 suggest that the intensity of the $^1\Sigma^+_u \leftarrow {}^1\Sigma^+_g$ absorption of linear C_3 should be distributed over a quite large energy range. Thus, the spectral feature observed by Chang and Graham might be part of a still broader absorption band. The position of the $^1\Sigma^+_u \leftarrow {}^1\Sigma^+_g$ band system can also be estimated from trends of the homologous series of electronic absorption spectra of linear carbon chains C_{2n+1} ($n = 2-7$) in neon matrixes, which were measured by Maier and co-workers. An extrapolation would yield a wavelength for the $^1\Sigma^+_u \leftarrow {}^1\Sigma^+_g$ transition of C_3 near 1700 Å.[25]

To investigate this strong and thus important transition of C_3 in more detail, we performed vacuum ultraviolet spectroscopy of the matrix-isolated carbon species both in argon and neon using synchrotron radiation. In addition, in a theoretical part of our contribution, we try to interpret the data and give an at least preliminary explanation of the basic structure of the observed absorption band system.

2. Experimental Section

2.1. Spectroscopic Instrumentation. Our measurements were carried out at the storage ring DORIS III at Desy (HASYLAB) in Hamburg. The setup of the HIGITI station is dedicated for optical spectroscopy of matrix isolated species using synchrotron radiation in the wavelength range from 400 to 5600 Å and is optimized in radiation intensity and spectral resolution between 600 and 2500 Å (resolution 0.3−10 Å). In our experiment, transmission spectra are limited to 1150 Å because of the absorption of the MgF_2 substrate, whereas for emission spectra, the absorption of the rare gas matrix (neon or argon) defines the lowest detectable wavelength.

This station was described in detail in ref 26 (see Figure 1). In brief, synchrotron radiation is dispersed by a primary monochromator. Several filters (MgF_2, quartz, and BK7) select a wavelength range and cut radiation of higher order grating reflections. After passing the MgF_2 substrate (SH), the radiation hits a BK7 viewport which is coated toward the inside of the chamber with sodium salicylate to convert the radiation $\lambda <$ 3000 Å into visible light. An external photomultiplier (TR) detects the converted radiation and thus indirectly monitors the transmitted synchrotron light.

Optical spectra can be recorded with three different systems. The primary monochromator which disperses the synchrotron radiation was used for measuring transmission spectra of the sample in the spectral range of 1150−5600 Å with a resolution up to 0.3 Å, a Seya-Namioka monochromator (resolution 2.5−150 Å) which covers the vacuum-ultraviolet (VUV) to ultraviolet (UV) wavelength range between 1100 and 3000 Å, and a Spex monochromator (resolution > 3 Å) for the ultraviolet to visible range (2000 and 9000 Å; Detection: photomultiplier or liquid nitrogen cooled CCD array). The latter two instruments were employed for emission spectroscopy.

2.2. UHV Compartments and Experimental Procedures. Carbon vapor molecules were produced in a water-cooled UHV chamber by resistive heating of graphite rods using DC current (typically 120−180 A at 5−8 V).[18] The MgF_2 substrate was facing the rods at a distance of about 700 mm. To reduce the deposition of rest-gas molecules such as H_2O, CO, and CO_2 in the solid noble gas matrix, all parts of the source chamber were baked out at 120 °C before each experiment. For the same reason, the carbon rods were heated to temperatures close to the evaporation condition before sample preparation. A magneti-

cally borne turbo molecular pump in combination with a membrane pump system provided oil-free conditions and evacuated the carbon source to pressures smaller than 5×10^{-9} mbar.

Between the cluster source and matrix deposition-compartment, another chamber with a liquid-nitrogen-cooled shield was placed. A small aperture (diameter 7 mm) in the shield reduced the radiation transfer of the heated carbon rods to the cold substrate in the matrix chamber. A UHV valve separated the carbon cluster source and sample compartment.

The UHV matrix-deposition compartment was equipped with a He-flow cryostat, which was moveable and rotatable under UHV conditions ($p < 1 \times 10^{-9}$ mbar). At the cryostat tip, a sample holder with the MgF_2 substrate was located. The helium flow through the cryostat and in addition a resistance heater mounted on the cryostat just above the coldfinger were employed for temperature control (Lakeshore Temperature Controller model 330). Commercially available gases with a purity of 99.999% for argon and neon have been used for matrix preparation without further purification.

Carbon−argon matrixes were prepared by depositing argon at a rate of 1500−8000 Å/min and carbon vapor (produced under various conditions) onto the low-temperature substrate at 18 K for 10−80 min. We prepared samples for which the carbon cluster concentration was rather low (i.e., the molar rare-gas-to-carbon ratio was more than 1000). Under these conditions, mutual cluster−cluster reactions were small, and the matrix contained mainly the cluster distribution prevailing in the vapor. The deposition process was monitored by measuring absorption spectra.

Argon matrixes showed relatively low scattering at low deposition rates and at an elevated deposition temperature (18 K). These features may be related to the crystallization of solid argon.[27] After preparing the sample, the substrate was cooled to $T = 10$ K, where all spectra were taken. To investigate a possible correlated behavior of the known electronic transition $^1\Pi_u \leftarrow X\ ^1\Sigma^+_g$ of C_3 and the new band system at around 1700 Å, the sample was thermally annealed up to 34 K for several times. After each temperature step, the absorption features were recorded again at 10 K. By heating the samples, diffusion of smaller molecules in the matrix was possible, leading to reactions between carbon molecules and/or atoms. This molecular growth process forms larger and consumes smaller carbon species and thus changes the intensity of the observed absorption lines in the measured spectra.[28] A distinct intensity correlation of two spectral bands is a hint to a common molecular origin.

Neon matrixes were prepared by co-depositing neon at a rate of 4500 Å/min and carbon vapor onto the low-temperature substrate at 4.3 K for nearly 60 min. Neon matrixes showed less scattering in the vacuum UV than argon matrixes. Sample preparation conditions were chosen so that the absorption of C_3 was the dominant feature in the recorded spectra.

To check for vacuum ultraviolet absorption features of contaminating molecules in the matrix, we inserted fresh graphite electrodes into our evaporator and outgassed the rods up to our standard evaporation temperatures. The progression of the CO A $^1\Pi \leftarrow X\ ^1\Sigma$ transition was the dominant band system. Careful outgassing of the graphite electrodes prior to experiment reduced the CO absorption to an extent, where monitoring the CO absorptions became difficult.

3. Experimental Results and Discussion

3.1. Vacuum, Ultraviolet, and Visible Carbon Cluster Absorptions. Absorption bands of argon and neon matrix-isolated carbon clusters are shown in Figures 2 and 3, respectively. These figures are an overview of spectra recorded in different wavelength ranges, merged, and background corrected. For wavelengths larger than 2000 Å, the absorption features in argon are in good agreement with spectra reported by different other groups.[29−34] Our data for the first time show the entire $^1\Sigma^+_u \leftarrow {}^1\Sigma^+_g$ absorption feature of C_3 centering at around 1700 Å in argon and 1600 Å in neon. The fraction of this band system between 1700 and 1890 Å was already observed by Chang and Graham in an argon matrix at 8 K.[22] However, the whole band system extends much further into the vacuum UV, at least to about 1400 Å. When samples were produced under different conditions, we noticed that the additional spectral features between 1400 and 1300 Å correlated in intensity with the 1600/1700 Å band system. This observation suggested that C_3 might also be the carrier of the bands in the 1400−1300 Å region, which perhaps belong to Rydberg states. The excitation energy of the ($1\pi_u \rightarrow 3s$) states $^3\Pi_u$ and $^1\Pi_u$ were calculated to be at 9.35 (1330) and 9.51 eV (1303 Å) respectively.[21]

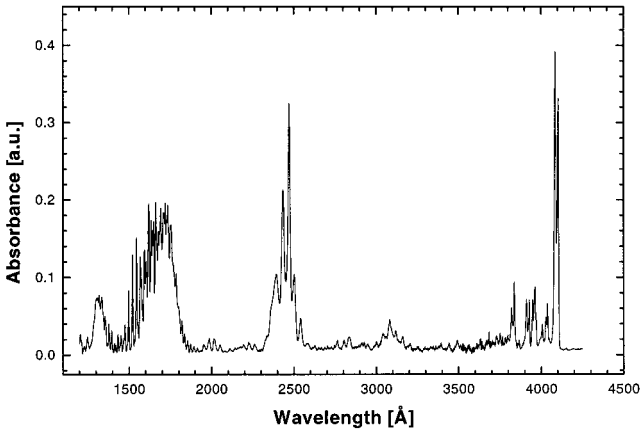

Figure 2. Electronic absorption spectrum of carbon vapor trapped in solid argon at 10 K in the vacuum ultraviolet−visible wavelength range. The band systems around 4100 and 3080 Å are assigned to the carbon clusters C_3 and to linear C_9, respectively. The strong feature near 2470 Å is a superposition of an absorption of C_2 (Mulliken system) and of linear C_6. The structured and broad absorption pattern between 1400 and 1900 Å originates from the electronic transition $^1\Sigma^+_u - X\ ^1\Sigma^+_g$ of C_3. The spectrum is recorded at a resolution of 1 Å in the VUV and was background-corrected for clarity.

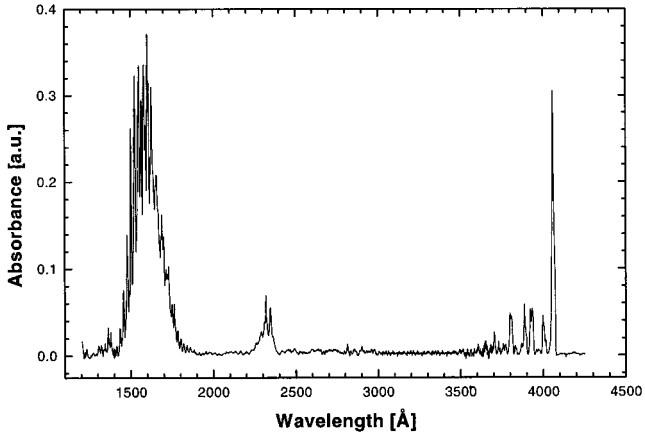

Figure 3. Electronic absorption spectrum of carbon vapor trapped in solid neon at 4.3 K in the vacuum ultraviolet−visible wavelength range. Because of the high dilution (Ne/C > 2500), the spectrum reflects more closely the carbon cluster distribution of our carbon source. The two electronic transitions of C_3 at 1600 and 4070 Å are the dominant features.

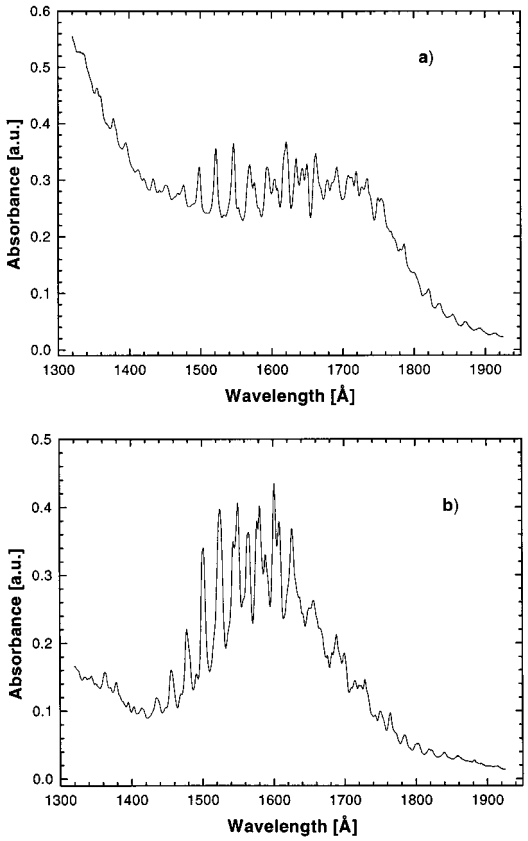

Figure 4. Absorption spectra of the C_3 ($^1\Sigma^+_u - X\ ^1\Sigma^+_g$) system (a) in solid argon at 10 K and (b) in solid neon at 4.3 K. The spectra are recorded at a resolution of 1 Å, and no background correction was applied.

Under the deposition conditions chosen, the clusters embedded in argon show a higher degree of molecular coagulation, i.e., show spectral features belonging to carbon clusters larger than C_3. There are weak bands of the species linear C_9 (at around 3100 Å, see ref 29) and linear C_6 (the band system around 2400 Å, see ref 30) upon which the Mulliken band of C_2 at 2380 Å (see ref 34) is superposed. The argon matrix spectra exhibit a broad structure at 1320 Å which has no direct counterpart in the neon data but might be assigned to the already mentioned Rydberg states of C_3.

In neon matrixes, the C_3 features are most prominent (Figure 3). Known spectral bands of other carbon molecules are either weak or could not be observed. Next to the established electronic transition $^1\Pi_u \leftarrow X\ ^1\Sigma^+_g$ of C_3 near 4070 Å, a broad band system of linear C_6 at 2300 Å occurs on which the Mulliken band of C_2 at 2320 Å is superposed, besides a shift in wavelength just like in argon, however, with much lower intensity. The dominant absorption around 1600 Å represents the $^1\Sigma^+_u \leftarrow X\ ^1\Sigma^+_g$ transition of C_3. It is seen again in both, argon (Figure 4a) and neon (Figure 4b) matrixes, at a resolution of 1.0 Å and without background correction. The influence of the different matrix materials on the spectral feature of C_3 can be recognized. For the convenience of the reader, a list of wavelengths (wavenumbers) of the bands is given in Table 1a in solid argon and Table 1b in solid neon. It is well-known that the matrix effects in neon are less severe, and compared to argon matrixes, the spectra in neon are more like the spectra in the gas phase. Thus, we think that the spectra obtained in neon are superior in quality to those in argon. Furthermore, our data may help to locate specific vibronic transitions for closer examination by high-resolution gas-phase spectroscopy.

TABLE 1: Positions of Observed Band Maxima of the $^1\Sigma^+_u \leftarrow X^1\Sigma^+_g$ System in Solid Argon at 10 K and Solid Neon at 4.3 K[a]

λ[Å]	ν[cm^{-1}]	λ[Å]	ν[cm^{-1}]	λ[Å]	ν[cm^{-1}]
A. Peaks in the Argon Matrix					
1913	52274	1707	58582	1522	65703
1892	52854	1692	59102	1499	66711
1872	53419	1685	59347	1491	67069
1855	53908	1678	59595	1476	67751
1837	54437	1669	59916	1468	68120
1821	54915	1662	60169	1451	68918
1801	55525	1650	60606	1442	69348
1787	55960	1643	60864	1434	69735
1781	56148	1635	61162	1421	70373
1773	56402	1620#	61728#	1413	70771
1769	56529	1609	62150	1395	71685
1764	56689	1604	62344	1382	72359
1754	57013	1594	62735	1378	72569
1749	57176	1583	63171	1360	73529
1738	57537	1576	63452	1355	73801
1735	57637	1569	63735	1338	74738
1727	57904	1553	64392	1319	75815
1720	58140	1547	64641		
1713	58377	1533	65232		
B. Peaks in the Neon Matrix					
1859	53792	1676	59666	1501	66622
1840	54348	1668	59952	1492	67024
1823	54855	1662	60169	1482	67476
1818	55006	1657	60350	1478	67659
1802	55494	1649	60643	1469	68074
1784	56054	1642	60901	1456	68681
1772	56433	1637	61087	1435	69686
1764	56689	1632	61275	1415	70671
1756	56948	1626	61501	1403	71276
1750	57143	1620	61728	1396	71633
1743	57372	1609	62150	1379	72516
1733	57703	1602#	62422#	1370	72993
1729	57837	1593	62775	1363	73368
1724	58005	1589	62933	1350	74074
1720	58140	1581	63251	1344	74405
1715	58309	1577	63412	1335	74906
1709	58514	1565	63898	1326	75415
1700	58824	1551	64475	1321	75700
1694	59032	1544	64767	1310	76336
1688	59242	1525	65574	1304	76687
1682	59453	1516	65963		

[a] A # indicates the band at which the absorptions (Figure 4) have a maximum.

3.2. Correlation of Excitation and Absorption Spectra. We searched for new C_3 emission bands but could only detect the well-known, strong a $^3\Pi_u \rightarrow X\ ^1\Sigma^+_g$ phosphorescence transition of C_3 at 5900 Å. Phosphorescence could be induced resonantly by excitation of the A $^1\Pi_u$ state of C_3, and also by excitation of the broad VUV absorption band around 1700 Å. This experimental result suggests that an excitation of the $^1\Sigma^+_u \leftarrow X\ ^1\Sigma^+_g$ transition results in an intersystem crossing into the triplet manifold of states. Nonradiative electronic relaxation then seems to lead to a population of the vibronic ground level of the triplet states including the a $^3\Pi_u$ state. The detailed mechanism of this later process remains to be investigated. In any event, the relaxation of the a $^3\Pi_u$ state to the X $^1\Sigma^+_g$ ground state can be observed as phosphorescence at 5900 Å.[13,18] In matrix-relaxation studies, the efficient intersystem crossing and internal conversion were also observed for various other small molecules, e.g., C_2 or NH.[35,36]

The HIGITI station allowed us to record the emission of excited molecules simultaneously in two different wavelength ranges, while scanning over the 1700 Å feature and monitoring the transmission spectrum. The SEYA spectrometer was used to record the emission signal of carbon monoxide, which is the

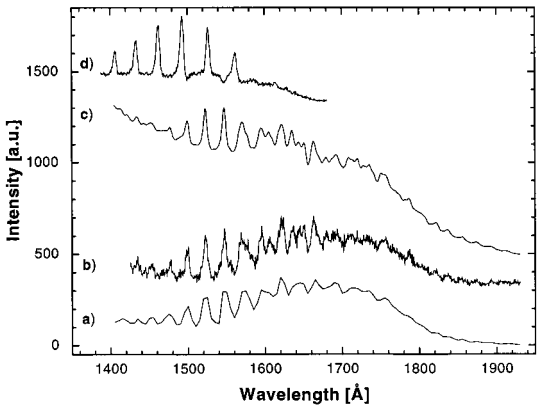

Figure 5. Absorption and excitation spectra of carbon vapor in an argon matrix. That the observed VUV absorption is the ($^1\Sigma^+_u - X\ ^1\Sigma^+_g$) transition of C_3 molecule is suggested by the agreement of the vacuum ultraviolet absorption (c) and the excitation spectrum of the known phosphorescence a $^3\Pi_u - X\ ^1\Sigma^+_g$ of C_3 at 5900 Å. In trace a, the C_3 phosphorescence was measured by a CCD array, and in b, it was measured by a photomultiplier. The excitation function of the CO phosphorescence (Cameron system) around 2150 Å (resolution 150 Å) was also monitored to check for a possible contribution of the CO absorption to the C_3 spectrum in the vicinity of 1500 Å (d). The contributions of CO appear to be negligible.

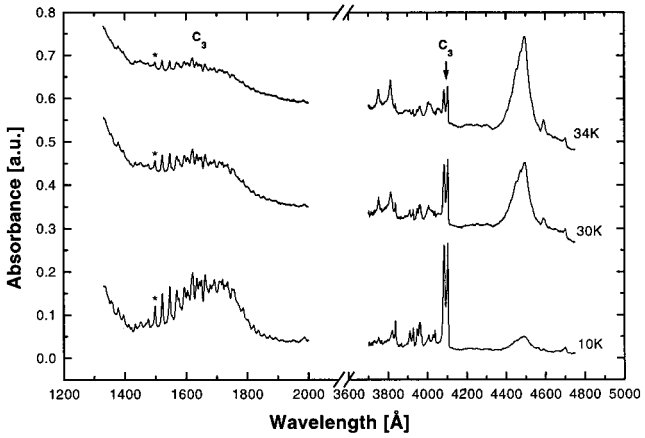

Figure 6. Absorption spectra of carbon clusters in argon at 10 K before and after annealing to 30 and 34 K. All spectra were recorded at 10 K. The two upper curves are shifted vertically for clarity. The thermally activated diffusion results in cluster−cluster reactions and molecular growth. The band of C_3 at 4100 Å and the broad VUV structure around 1700 Å show a correlated decrease, whereas other absorption features, belonging to larger carbon molecules, increase. The band at 4500 Å probably originates from linear C_{15} (ref 25).

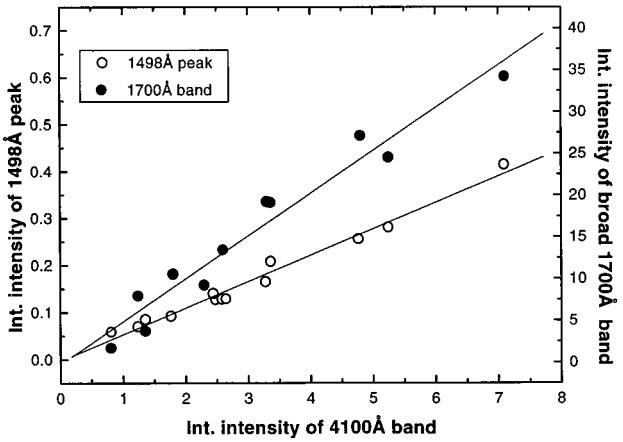

Figure 7. Correlation plot of the integrated absorptivities of the C_3 band system at 4100 Å versus that of a single narrow peak at 1498 Å and the entire broad 1700 Å system, respectively. The narrow peak is marked by an asterix in Figure 6.

main potential contamination in our spectra. The progression of the CO $A\ ^1\Pi \leftarrow X\ ^1\Sigma$ transition extended from 1560 to 1310 Å in argon and could interfere with the C_3 band system. To detect the features belonging to CO, the Seya monochromator was set to 2150 Å (with a resolution of 150 Å) in order to record the phosphorescence signal of the a $^3\Pi \rightarrow X\ ^1\Sigma$ progression of CO (Cameron system), which is excited by the $A\ ^1\Pi \leftarrow X\ ^1\Sigma$ transition. To monitor the phosphorescence of C_3, the Spex monochromator was set to 5900 Å (resolution 18 Å), and the intensity was monitored either with a CCD array or a photomultiplier (see Figure 1). By this method, the vacuum ultraviolet excitation spectra (which should reproduce the absorption spectra apart from a scaling factor) of both carbon monoxide and C_3 could be detected simultaneously and from the same matrix. Our data are displayed in Figure 5 and show definitely that the strong and sharp excitation (absorption) bands at around 1500 Å, which on first glance might be associated with CO, are in fact originating from C_3. The C_3 excitation spectrum correlates well with the transmission spectrum measured simultaneously in the same wavelength range.

3.3. Correlation of Absorptions by Matrix Annealing Experiments. Figure 6 shows absorption spectra of carbon vapor in argon matrixes taken in two wavelength ranges. The temperature dependence of carbon cluster aggregation was tested by annealing. After deposition, the sample was heated to temperatures of 28, 30, 32, and 34 K for about 10 min, while spectra were recorded at 10 K after each annealing step. For clarity, only three spectra are shown here vertically shifted. The lowest spectrum was measured after the deposition; the two others were measured after annealing to $T = 30$ and 34 K, respectively. In the wavelength range of 3700−4750 Å, the characteristically shaped $^1\Pi_u \leftarrow X\ ^1\Sigma^+_g$ "cometary" absorption band of C_3 around 4100 Å decreases in intensity during the thermal treatment of the sample. The broad absorption between 1350 and 1900 Å shows a similar behavior and supports an assignment to C_3. To establish the degree of correlation for the two features, the peak heights (or integrated intensities) are plotted against each other. A positive correlation should result in a straight line with an intercept at zero. For this purpose, the spectra of samples produced under various conditions were studied. Different initial cluster distributions and concentrations in the argon matrix were obtained, for example, by changing the DC power of the evaporation process and changing the argon deposition rate. In total, there were two annealing runs with nine data points and a few samples without thermal treatment at our disposal. First, we plotted the integrated intensity of the known C_3 absorption at 4100 Å versus the integrated intensity of the entire VUV C_3 absorption feature ("1700 Å band" in Figure 7) which we placed between 1427 and 1846 Å, assuming a linear baseline between these points. The experimental points scatter around the straight line fit. The correlation can be improved when a nonlinear background is introduced which better accounts for the scattering of the matrix. Therefore, we investigated also narrow peaks, e.g., at 1498 (shown by an asterix in Figure 6) 1522, and 1547 Å. The data of the 1498 Å absorption are displayed in Figure 7. The correlation coefficients were calculated as 0.98 for all three bands, and the intercept was consistently zero. These data again support the assignment of the band as the $^1\Sigma^+_u - X\ ^1\Sigma^+_g$ transition of C_3.

3.4. VUV Absorption Band System. Our assignment of this band to the $^1\Sigma^+_u \leftarrow X\ ^1\Sigma^+_g$ transition of C_3 is in good agreement with the available quantum chemical calculations.[19−21] Römelt

at al.[21] estimate that the $^1\Sigma^+_u$ state is located about 8 eV above the ground state. This value corresponds to 1550 Å which is close to the observed $^1\Sigma^+_u \leftarrow X\ ^1\Sigma^+_g$ band center. These authors conclude that the antibonding character of this excited state leads to a potential minimum at slightly larger C−C bond length, i.e., at 1.390 Å compared to 1.308 Å in the $^1\Sigma^+_g$ ground-state. Furthermore, potential curves for the symmetric and asymmetric C−C stretch and for the C−C−C bending in the $^1\Sigma^+_u$ state were calculated in ref 21. The results indicate the presence of a bound linear configuration, i.e., a local minimum at zero bending. The potential curve as a function of bending angle is M-shaped i.e., exhibits a local minimum at 0° in the middle of the M (linear case) but also two genuine outer minima at finite bending angles. These latter minima originate from an avoided crossing of the potential curve with that of a lower lying Π_g state. This result would imply that C_3 should be bent in the vibrational ground level of the $^1\Sigma^+_u$ state. The predicted symmetric stretching frequency is quite similar to that of the ground state, i.e., $\nu_1 = 1235\ cm^{-1}$. The antisymmetric stretching frequency ν_3 is estimated to be "considerably larger", and no bending mode frequency is given. More recently, Grimme and Peyerimhoff [37] again calculated the $^1\Sigma^+_u$ and adjacent excited C_3 states, applying the TD-DFT method. The new data show that the potential curve of the $^1\Sigma^+_u$ state is more likely W-shaped, i.e., shows no minimum at zero bending but rather declines with increasing bending angle, thereby approaching a lower lying $^1\Pi_g$ and leading to an avoided crossing type of minimum feature in the energy surface. Our own MR-AQCC calculation support this finding (see below).

A closer examination of the absorption feature (Figure 4, in particular 4b) shows relatively clear progressions at the red and blue portion of the absorption feature. In the central part, both progressions appear to be superimposed in an irregular fashion, and also additional progressions seem to complicate the spectrum. We tried to find further periodicity in the spectrum by applying several numerical techniques, but these attempts remained unsuccessful.

The progression at the blue wing of the absorption band extends to 1546 Å in the red and probably beyond, but because of superposition with other peaks, this progression is less clear. The first two peaks at the blue side are spaced by 985 cm^{-1}, and the spacing toward the red increases to 1099 cm^{-1} probably because of anharmonicities of the potential curve. An extrapolation of the frequency data to further peaks in the red leads to a rather tentative band origin at about 1581 Å in neon (1605 Å in argon). In view of the complexities of the central portion of the absorption spectrum, we were not attempting a band analysis and a search for band origins which we think would probably give no meaningful results. We instead try to reproduce the basic pattern of the entire spectrum by quantum chemical calculations of synthetic absorption spectra, as will be reported in the following chapter. From these data, it appears that the above progression should extend much further into the red, and in fact, there are wiggles discernible which are reaching up to 1780 Å in the observed spectrum. We conclude that the progression at the blue wing with an average spacing of about 1100 cm^{-1} fits well to the theoretically predicted figure[21] of the ν_1 mode; that is, it very likely belongs to the symmetric stretch.

The long progression starting from about 1859 Å in the red portion and extending to a wavelength smaller than 1635 Å in neon (1892−1670 Å in argon) has a spacing of about 550 cm^{-1} and may be attributed to a bending vibration. There are various irregularities apparent in this progression, e.g., at around 1820, 1740, and 1720 Å, which seem to indicate a complex bending

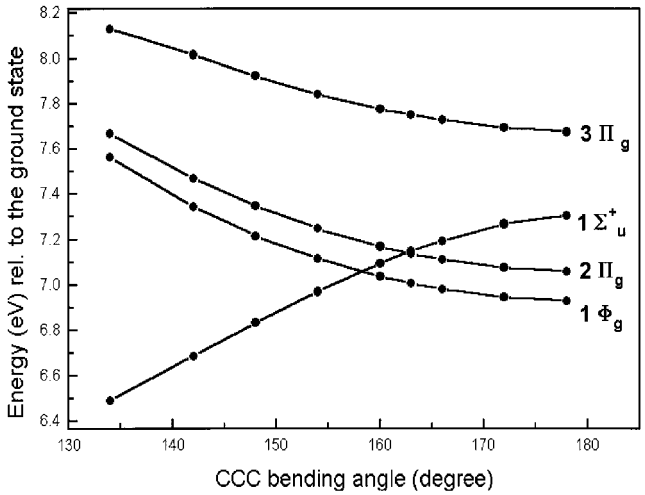

Figure 8. Electronic energies of the states of concern as a function of the bending coordinate. The calculations were performed with a fixed C−C bond length of 1.4049 Å. Only the components with B_2 symmetry are shown. Notice the crossing of levels (for details, see text).

potential. Strongly varying vibronic couplings between the $^1B_2$ components of the $^1\Sigma_u$ and the adjacent $^1\Pi_g$ states (notice the divergence of the B_2 states originating from $^1\Sigma_u$ and $3^1\Pi_g$ in Figure 8) and an avoided crossing type of energy minimum in the energy surface may be responsible for these complications.

Comparing the progressions at the red and blue portion of the band system in both matrixes, one finds a one-to-one relation between the bands in argon and neon. However, it is difficult to correlate the bands observed in both matrixes through the entire absorption feature. Apparently, the two matrixes have a different influence on the spectral features of C_3. We think that the peak group at 1565, 1602, 1609, and 1626 Å in neon and 1594, 1635, 1643, and 1662 Å in argon resemble each other because these are similar in shift and peak shape.

For a further discussion, we should consider the low temperatures prevailing in our matrixes. Under these conditions, all electronic transitions originate from the lowest vibrational level ($v'' = 0$) of the totally symmetric $^1\Sigma^+_g$ ground-state. Let us assume that C_3 remains linear in the electronically excited state as for example was done in the early work of Chang and Graham.[22] In the $^1\Sigma^+_u \leftarrow X\ ^1\Sigma^+_g$ absorption spectrum, one expects only progressions of the symmetric stretch vibration to occur. The other possible vibrations of odd (u) symmetry should be absent for symmetry reasons. However, their even overtones (with $v' = 2$, 4, and 6) have even (g) symmetry and may occur. Chang and Graham assigned the weak progression at the red wing of the absorption to the progression of even overtones of the bending vibration and obtained a fundamental frequency of about 300 cm^{-1} from their data in argon matrixes.[22] In view of the recent theoretical results, however, this interpretation has to be modified. There are electronic states with $^1\Pi_g$ symmetry in close vicinity (0.2−0.4 eV, see Figure 8) of the $^1\Sigma^+_u$ level which can interact with the $^1\Sigma^+_u$ state via vibronic coupling and can lead to the excitation of the bending mode (π_u) in the electronically excited $^1\Sigma^+_u$ state. In other words, because of the vibronic interaction, C_3 becomes bent (C_{2v}) in the electronically excited $^1\Sigma^+_u$ (respectively B_2) state which implies that transitions to all levels of the bending mode (totally symmetric species a_1) become electronically allowed. The 550 cm^{-1} progression may thus be directly related to a usual progression in such a bending mode, rather than to a progression of only the even overtones of that mode. A bending frequency of 550 cm^{-1} is surprisingly large. Both, the stabilization of C_3 by bending and the presence

TABLE 2: Calculated Vertical Excitation Energies (eV) (Oscillator Strength in Parentheses) of the Low-Lying Valence States of C_3[a]

state	character	MCSCF	MR−CI	MR-AQCC
$1^1\Pi_u$	$\sigma_u \rightarrow \pi_g$	3.41	3.22	3.11 (0.02)
$1^1\Sigma_u^-$	$\pi_u \rightarrow \pi_g$	3.91		3.98
$1^1\Delta_u$	$\pi_u \rightarrow \pi_g$	3.91	4.02	4.02
$1^1\Pi_g$	$\sigma_g \rightarrow \pi_g$	4.06	4.04	4.00
$1^1\Phi_g$	$\sigma_u, \pi_u \rightarrow \pi_g, \pi_g$	7.42	7.20	7.04
$2^1\Pi_g$	$\sigma_u, \pi_u \rightarrow \pi_g, \pi_g$	7.73	7.26	7.20
$3^1\Pi_g$	$\sigma_u \rightarrow \pi_u$	8.22	7.91	7.89
$1^1\Sigma_u+$	$\pi_u \rightarrow \pi_g$	10.01	8.38	7.97 (0.94)
$2^1\Pi_u$	$\sigma_g, \pi_u \rightarrow \pi_g, \pi_g$	8.47	8.05	7.71 (0.00)
$1^1\Phi_u$	$\sigma_g, \pi_u \rightarrow \pi_g, \pi_g$	8.58	8.39	8.36
$2^1\Sigma_u+$	$\sigma_u, \pi_u, \pi_u \rightarrow \pi_g, \pi_g, \pi_g$	9.66	9.71	9.55

[a] Calculations have been performed at the experimental equilibrium geometry (1.2936 Å).[47] The 8 × 8 CAS reference space with orbitals $4\sigma_g$, $3\sigma_u$, $1\pi_u$, $1\pi_g$, and $2\pi_u$ has been used. The basis set was cc-pVTZ.

of electrons in the higher π orbitals may be responsible for the stiff bending behavior of the excited molecule. The latter feature was already noticed in the well studied $^1\Pi_u$ state of C_3 (see, e.g., ref 3).

As a further consequence of vibronic coupling, excitation to the $^1\Pi_g$ states can "borrow" intensity and thus contribute to the absorptions in the observed spectrum. We think that such "borrowing" effects may, to some extent, be responsible for the complex pattern of bands one can notice in the central portion of the absorption feature.

Our measurements showed no additional fluorescence emerging from the excited $^1\Sigma^+_u$ state. Apparently, efficient radiationless relaxation and an intersystem crossing into the triplet manifold of C_3 takes place. The theoretical results presented in the following suggest at least in part an explanation for this observation. Calculations of the energy surfaces predict a funnel like feature, i.e., a close approach (avoided crossing or conical intersection) of the states originating from $^1\Sigma^+_u$ and $2^1\Pi_g$ at about 163° bending angle (see Figure 8). As a consequence, the Born−Oppenheimer approximation must break down at around this configuration, and photoexcited C_3 will, via nuclear vibrations, efficiently reach lower levels, from which further radiationless relaxation seems to occur.

4. Theoretical Analysis of the VUV Band

As described in the experimental part, all doubts concerning the origin of the observed absorption have been removed, and the band is attributed entirely to the C_3 moiety. In this section, we present theoretical results which intend to help in the assignment and understanding of this band. For comparison with the experiment, we concentrate on the C_3 spectrum observed in neon.

To obtain accurate theoretical data, the method used to describe the electronic structure has been chosen very carefully. First, preliminary model calculations were performed which show that there are several excited states overlapping in energy with the measured spectrum. A qualitative characterization of these states is given in Table 2.

It is seen from the table that some of these states are doubly excited, so multireference type methods need to be used. To include also dynamical correlation, which is necessary if accurate excitation energies are required, MR−CI-type methods seem to be the best choice. The accuracy of MR−CI-type methods for excited states has been investigated recently by Müller et al.[38] on diatomic molecules including C_2. It has been concluded that the error of the MR−CI method because of the well-known size extensivity error is substantial, and the use of MR−CI with Davidson correction[39,40] or approximately extensive versions such as MR-AQCC (multireference averaged quadratic coupled cluster)[41,42] is necessary to obtain reliable results. These authors concluded that the error of T_e obtained by the MR-AQCC method using a valence CAS (complete active space) reference space is about 200−300 cm^{-1} only if the basis set error is eliminated by extrapolation. Relevant for this study is that the error was only about 500−600 cm^{-1} with the moderate triple-ζ correlation consistent (cc-pVTZ) basis by Dunning et al.[43,44] when only valence states were considered.

For C_3, the use of the full valence CAS reference space is not practical. Instead, the reference space has been selected to reach a balanced description of the states of interest, i.e., the $1^1\Sigma_u$, $2^1\Pi_g$, $1^1\Phi_g$, and $3^1\Pi_g$ states. In this process, several reference spaces have been compared, and the following has been selected for further calculations: eight electron six orbital CAS including the $4\sigma_g$, $1\pi_u$, $1\pi_g$, and $1\sigma_u$ orbitals augmented by single excitation to the $5\sigma_g$ and $2\pi_u$ orbitals. All single and double excitations out of these reference functions have been considered in the subsequent MR-AQCC calculations except that the three MOs corresponding to the core orbitals have been kept doubly occupied. This type of wave function included about 6−7 million configurations depending on the symmetry of the states. We expect a somewhat larger error than with a full valence CAS. The error in the excitation energies can be estimated by comparing results obtained by different reference spaces and by the MR−CI and the MR-AQCC methods to be about 2000−3000 cm^{-1}.

We used the cc-pVTZ atomic basis set in all calculations. We did not include diffuse functions because Rydberg states are higher in energy than the ones investigated in this study. The orbitals were obtained from state-averaged MCSCF calculation based on a eight electron and nine orbital CAS wave function including the $4\sigma_g$, $1\pi_u$, $1\pi_g$, $1\sigma_u$, $5\sigma_g$ and $2\pi_u$ orbitals, as mentioned above. The averaging included the $^1\Sigma_g^+$ ground state, the two lowest $^1\Sigma_u^+$ states, the four lowest $^1\Pi_g$ states, and a $^1\Phi_g$ state. The Columbus program system was used in all calculations.[45]

From the states in Table 2, excitations to the $1^1\Sigma_u^+$, $1^1\Pi_u$, and $2^1\Pi_u$ states are optically allowed. The calculated transition moment for the later is, however, very small, and therefore, one expects a negligible contribution from the $2^1\Pi_u$ state to the spectrum. This can easily be understood qualitatively also, because this state is dominated by a double excitation from the ground state. Therefore, the observed VUV band can be safely identified with a transition from the ground state to the $1^1\Sigma_u^+$ state. This assignment is in agreement with the previous suggestions of Chang and Graham[22] and the theoretical predictions of Römelt et al.[21]

According to group-theoretical-based selection rules, the absorption band corresponding to the excitation $1^1\Sigma_u^+ \leftarrow 1^1\Sigma_g^+$ should show progressions corresponding to vibrations of g (even) symmetry, e.g., the symmetric stretching vibration, or possibly even overtones of the other u (odd) modes in the excited state. A spectrum based on the theoretical data (see below) and using Franck−Condon-type analysis is seen in Figure 9 (the case $\Lambda = 0$). The synthetic spectrum shows a vibrational progression similar to that observed on the high energy side of the experimental absorption feature. However, the somewhat irregular progressions observed on the low energy side are not reproduced, indicating that some other interactions must influence the spectrum. As has been pointed out already in ref 21, such interaction is possible with states of Π_g symmetry via the C−C−C bending vibration. The group theoretical restriction

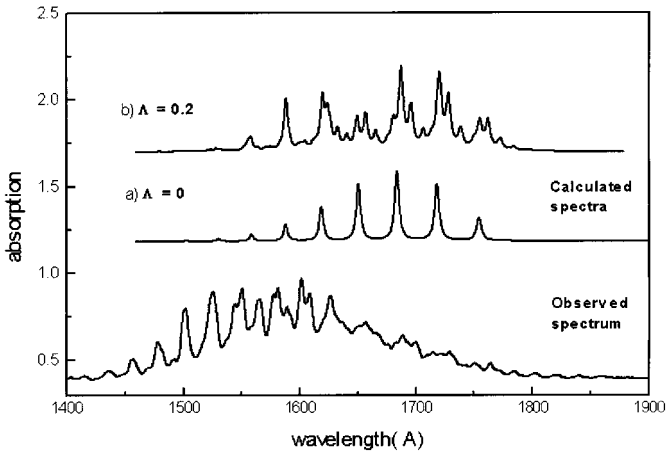

Figure 9. Simulated VUV C_3 spectra compared with the experimental data (neon matrix, see Figure 3). Calculations were carried out for various interstate coupling parameters Λ ($\Lambda = 0$ means no coupling) under the simplifying assumption that only the adjacent $3\Pi_g$ state (see Figure 8) couples. Notice that (apart from the absolute position of the band system) the synthetic spectrum can qualitatively reproduce some of the basic patterns of the experimental band system.

for these interactions is given by

$$\Gamma_{elec,1} \otimes \Gamma_{vib} \supset \Gamma_{elec,2}$$

where $\Gamma_{elec,1}$ and $\Gamma_{elec,2}$ are the species of the states coupled by the vibration of species Γ_{vib}. Using the species of the linear bending mode (Π_u), the equation is satisfied for the excited Π_g but not for the Φ_g states. There are two Π_g states close to the $1^1\Sigma_u^+$ state, so a closer investigation of the vibronic interaction is warranted. Considering the states in Table 2, we do not see any other possibility for vibronic coupling.

In a first step, we have calculated parts of the potential energy surface along the bending and stretching coordinate. Qualitatively, we reached similar conclusions as the authors of ref 37. With respect to the stretching coordinate, the surface shows a distinct minimum at the linear configuration. With respect to the bending coordinate, the results are shown in Figure 8. Clearly, the energy of the $1^1\Sigma_u^+$ state decreases with bending; a feature which implies that the $1^1\Sigma_u^+$ energy surface exhibits a saddle point at the linear geometry. The lowering of the energy upon bending can be explained by the interaction of the $1^1\Sigma_u^+$ state with one of the components of the $3^1\Pi_g$ state which has the same B_2 symmetry (in the bent form) as the $1^1\Sigma_u^+$. The picture is even more complicated by the presence of the $2^1\Pi_g$ state which appears to cross the $1^1\Sigma_u^+$ curve at a bending angle of about 163°.

To gain more insight, we applied the simple linear vibronic interaction model developed by Köppel and co-workers,[46] and it appears that a qualitative understanding of the observed complicated vibrational structure can be obtained when vibronic coupling is taken into account. In the linear vibronic coupling model[46] the vibronic Hamiltonian is expanded around the symmetric (linear) geometry using the vibrational normal coordinates of the ground state. The intrastate coupling parameter (κ_i) of the individual states is essentially the derivative of the energy of the excited state along the symmetric normal coordinate, whereas the interstate coupling parameter for the vibronically coupled excited states λ_{ij} describes the interaction of the states along the antisymmetric (in our case bending) coordinates. The ground-state properties entering the vibronic coupling model are given in Table 3, whereas the parameters of the excited states are listed in Table 4. The simulation of the spectrum has been performed with the *xsim* program of Sattelmayer and Stanton[48] which has been modified for the treatment of linear molecules.

TABLE 3: Ground State Properties of C_3[a]

	MR-AQCC	expt (ref 47)
r_e (Å)	1.3027	1.2936
ω_e (stretching) cm^{-1}	1196	1206
ω_e (bending) cm^{-1}	387	65[b]
total energy (hartree)	−113.83316	

[a] Calculations have been performed at the MR-AQCC level (see text for details) using the cc-pVTZ basis. [b] Anharmonic value.

TABLE 4: Calculated Parameters for the Linear Vibronic Model[a]

state	$1\Sigma^+_u$	$2^1\Pi_g$	$1^1\Phi_g$	$3^1\Pi_g$
vertical excitation energy (eV)	7.43	7.19	6.95	7.53
$\partial E/\partial q_{stre}$ (eV)[b]	0.3270	0.2696	0.2577	0.0525

[a] Calculated at the theoretical ground-state equilibrium geometry (1.3027 Å). Calculations have been performed at the MR-AQCC level (see text for details) using the cc-pVTZ basis. [b] Derivative of the energy according to the symmetric stretching normal coordinate (dimensionless) of the ground state.

The ground-state bond length and the symmetric stretching harmonic frequency are in good agreement with the experiment and other predictions from theory.[47] The accuracy is in line with that obtained for C_2 using the cc-pVTZ basis.[38] The bending frequency, however, is significantly larger than the one determined from the experiment. As shown by Mladenovic et al.,[47] this quantity is very sensitive to the basis functions, and diffuse functions are absolutely necessary to get reliable results. Because our goal is the description of the excitation spectrum rather than that of the ground state, we have not pushed the calculation any further, especially because this bending mode enters only in the expansion and its actual value should not influence the results.

The κ_i parameters have been calculated using the analytic derivative of the excited-state energy which then has been transformed to the normal coordinates. The λ_{ij} coupling for the $1^1\Sigma_u^+$ and $3^1\Pi_g$ states has been calculated from the potential energy curve of the two states along the bending coordinate assuming that their divergence is due to their vibronic interaction. To obtain the λ_{ij} coupling for the $1^1\Sigma_u^+$ and $2^1\Pi_g$ states, we have calculated the 3D potential energy surface of the two states around their assumed crossing using bending and symmetric stretching coordinates. It turned out that these surfaces do not cross exactly but come very close to each other: the energy difference is only about 50 cm^{-1} at 162.5° and 1.419

Å. We think we have here the situation of an "avoided crossing". In a two state model like the linear vibronic coupling model, the distance of the two surfaces is proportional to the interstate coupling parameter; in case of no coupling, the two states would be degenerate. In the situation considered here, the distance in energy is so small that the λ_{ij} value should be negligible. Therefore, we consider only the $^1\Sigma_u^+$ and the $3^1\Pi_g$ states in the simulations. Figure 9 shows the experimental spectrum compared to the obtained simulated spectra, (a) without interstate coupling, a case we already have discussed, and (b) with interstate coupling. Λ is the coupling parameter λ_{ik} between the considered states.

Although there are quite significant differences, the basic characteristics of the VUV band are clearly discernible in the simulated spectrum (b). On the high energy side of the synthetic spectrum where the coupling is small, there is an almost regular progression with an average spacing of 1200 cm^{-1}. In the experimental data, one can recognize a similar progression and thus identify these features with the v' progression of the symmetric stretching mode in the $^1\Sigma_u^+$ state. The other significant observation is the loss of regularity on the low energy side, both in the experimental and in the simulated spectrum. In this region, all vibrational transitions will contain some symmetric stretching and bending character because of the variable composition of the wave functions in the interacting states. Thus, the interpretation of the vibrational progression-like series on the high energy side as a v' symmetric vibration progression should also be handled with reservations. The other fact which prevents the usual assignment of the different lines to a given progressions is that on the potential energy surface of the $1^1\Sigma_u^+$ state there is no minimum which could be interpreted as the equilibrium structure for this state. The minimum in the vicinity of the avoided crossing between the $1^1\Sigma_u^+$ and $2^1\Pi_g$ states cannot be considered as such because of the breakdown of the Born−Oppenheimer approximation because of the very small separation of the two states. The starting edge for the band systems on the low energy side, however, agrees well between theory and experiment.

When considering the differences of the calculated and observed spectrum, one should, however, keep in mind the approximations of the model used in the calculations. The linear vibronic coupling model assumes an approximate form of the underlying (Born−Oppenheimer) surfaces obtained form the ab initio calculations, and therefore, the calculated vibrational levels are also biased by this approximation. We also expect the model to break down near the avoided crossing between the $1^1\Sigma_u^+$ and the $2^1\Pi_g$ surfaces. Because this point is a low energy point on the $1^1\Sigma_u^+$ surface, the effect of this breakdown influences the low energy part of the spectrum. Unfortunately, we are unable to predict the magnitude of this effect, although we assume that it is small because the avoided crossing is already far from the Franck−Condon region. A more reliable simulation of the spectrum would require going beyond the linear coupling model and perform dynamical calculations with three surfaces corresponding to the $1^1\Sigma_u^+$, $2^1\Pi_g$, and $3^1\Pi_g$ states. This would be a rather big undertaking, however, and therefore out of the scope of the present paper. Such an extended study is in progress. We hope that this will provide a better agreement with the experimental VUV spectrum and will allow us to explain all relevant features of the observed spectrum in more detail.

Conclusions

Using synchrotron radiation, the spectrum of the carbon molecule C_3 was investigated in the vacuum ultraviolet−visible wavelength range at a resolution up to 0.3 Å. In particular, we measured absorption spectra of the $^1\Sigma^+_u \leftarrow X\ ^1\Sigma^+_g$ transition of C_3 around 1600 Å in neon at 4.3 K and 1700 Å in argon at 10 K. Intensity correlations with the known electronic transition and the excitation spectrum of the $a\ ^3\Pi_u \rightarrow X\ ^1\Sigma^+_g$ phosphorescence emission of C_3 show that the VUV band system originates from the C_3 molecule. Our own data and the available quantum chemical data support the above assignment for the observed absorption. At the red and the blue portion of the observed absorption band system, simple progressions can be recognized, probably originating from bending and symmetric stretching vibrations, respectively, whereas the middle part of the band system shows a complex superposition of progressions. Our quantum chemical calculations of synthetic spectra show that the complexities in the observed spectrum at least in part come from interstate vibronic coupling between the $^1\Sigma^+_u$ state and the adjacent Π_g states. Furthermore, theoretical calculations suggest that the $^1\Sigma^+_u$ state is unstable upon bending, leading to an avoided crossing type of feature with the lower lying Π_g energy surfaces. The intersection of the energy surfaces and their effect on the resulting spectra remains to be investigated by more detailed future calculations.

Acknowledgment. The rather generous financial support by the Deutsche Forschungsgemeinschaft is gratefully acknowledged. The authors from Heidelberg thank I. Čermák (Chemnitz) for discussions and appreciate the help of S. Grimme (Münster) and S. Peyerimhoff (Bonn) for carrying out exploring quantum calculation. W.K. thanks A. L. Ong (Heidelberg) for his help in preparing the manuscript and T. Wakabayashi (Kyoto) for his many valuable comments. P.G.Sz. appreciates the stimulating discussions with H. Köppel. P.G.Sz. and L.N. acknowledge financial support for this work by the Hungarian OTKA Foundation under Contract Number T032549. P.G.Sz. thanks also for support by Grant T032980.

References and Notes

(1) Huggins, W. *Proc. R. Soc. (London)* **1882**, *33*, 1.
(2) Douglas, A. E. *Astrophys. J.* **1951**, *114*, 466.
(3) Weltner, W. Jr.; van Zee, R. J. *Chem. Rev.* **1989**, *89*, 1713.
(4) van Orden, A.; Saykally, R. J.*Chem. Rev.* **1998**, *98*, 2313.
(5) Motylewsky, T.; Linnartz, H.; Vaizert, O.; Maier, J. P.; Galazutdinov, G. A.; Musaev, F. A.; Krelowski, J.; Walker, G. A. H.; Bohlender, D. A. *Astropys. J.* **2000**, *531*, 312.
(6) Homann, K.-H. *Angew. Chem. Int. Ed.* **1998**, *37*, 2435.
(7) Kroto, H. W.; Heath, J. R.; O'Brien, S. C.; Curl, R. F.; Smalley, R. E. *Nature* **1985**, *318*, 162.
(8) Krätschmer, W.; Lamb, L. D.; Fostiropoulos, K.; Huffman, D. R. *Nature* **1990**, *347*, 354.
(9) Zavitsanos, P. D.; Carlson, G. A. *J. Chem. Phys.* **1973**, *59*, 2966.
(10) Skell, P. S.; Havel, J. J.; McGlinchey, M. J. *Acc. Chem. Res.* **1973**, *6*, 97.
(11) Barger, R. L.; Broida, H. P. *J. Chem. Phys.* **1962**, *37*, 1152.
(12) Weltner, W., Jr.; Walsh, P. N.; Angell, C. L. *J. Chem. Phys.* **1964**, *40*, 1299.
(13) Weltner, W., Jr.; McLeod, D., Jr. *J. Chem. Phys.* **1964**, *40*, 1305.
(14) Weltner, W., Jr.; McLeod, D., Jr. *J. Chem. Phys.* **1966**, *45*, 3096.
(15) Bondybey, V. E.; English, J. H. *J. Chem. Phys.* **1978**, *68*, 4641.
(16) Smith, A. M.; Agreiter, J.; Härtle, M.; Engel, C.; Bondybey, V. E. *Chem. Phys.* **1994**, *189*, 315.
(17) Peric-Radic, J.; Römelt, J.; Peyerimhoff, S. D.; Buenker, R. J. *Chem. Phys. Lett.* **1977**, *50*, 344.
(18) Čermák, I.; Förderer, M.; Kalhofer, S.; Stopka-Ebeler, H.; Krätschmer, W. *J. Chem. Phys.* **1998**, *108*, 10129.
(19) Pitzer, K. S.; Clementi, E. *J. Am. Chem. Soc.* **1959**, *81*, 4477.
(20) Williams, G. R. J. *Chem. Phys. Lett.* **1975**, *33*, 582.
(21) Römelt, J.; Peyerimhoff, S. D.; Buenker, R. J.*Chem. Phys. Lett.* **1978**, *58*, 1.
(22) Chang, K. W.; Graham, W. R. M. *J. Chem. Phys.* **1982**, *77*, 4300.
(23) Kalcher, J.; Janoschek, R. *J. Mol. Struct. (THEOCHEM)* **1991**, *80*, 509.
(24) Kolbuszewski, M. *J. Chem. Phys.* **1995**, *102*, 3679.

(25) Maier, J. P. *Chem. Soc. Rev.* **1997**, 21.
(26) Zimmerer, G. *Nucl. Instrum. Methods* **1991**, *A308*, 178.
(27) Schulze, W.; Kolb, D. M. *J. Chem. Soc., Faraday Trans.* **1973**, *70*, 1098.
(28) Grutter, M.; Freivogel, P.; Forney, D.; Maier, J. P. *J. Chem. Phys*. **1997**, *107*, 5356.
(29) Forney, D.; Freivogel, P.; Grutter, M.; Maier, J. P. *J. Chem. Phys*. **1996**, *104*, 4954.
(30) Grutter, M.; Wyss, M.; Riaplov, E.; Maier, J. P.; Peyerimhoff S. D.; Hanrath, M. *J. Chem. Phys.* **1999**, *111*, 7397.
(31) Krätschmer, W.; Sorg, N.; Huffman, D. R. *Surf. Sci*. **1985**, *156*, 814.
(32) Kurtz, J.; Huffman, D. R. *J. Chem. Phys*. **1990**, *92*, 30.
(33) Szczepanski, J.; Vala, M. *J. Phys. Chem*. **1991**, *95*, 2792.
(34) Milligan, D. E.; Jacox, M. E.; Abouaf-Marguin, L. *J. Chem. Phys.* **1967**, *46*, 4562.
(35) Bondybey, V. E. *J. Chem. Phys.* **1976**, *65*, 2296.
(36) Bondybey, V. E. *J. Chem. Phys.* **1976**, *65*, 5138.
(37) Grimme, S.; Peyerimhoff, S. D. unpublished data, 1998.
(38) Müller, T.; Dallos, M.; Lischka, H.; Dubrovay, Z.; Szalay, P. G. *Theor. Chem. Acc.* **2001**, *105*, 227.
(39) Langhoff, S. R.; Davidson, E. R. *Int. J. Quantum Chem.* **1974**, *8*, 61.
(40) Davidson, E. R.; Silver, D. W. *Chem. Phys. Lett*. **1977**, *52*, 403.
(41) Szalay, P. G.; Bartlett, R. J. *Chem. Phys. Lett*. **1993**, *214*, 481.
(42) Szalay, P. G.; Bartlett, R. J. *J. Chem. Phys*. **1995**, *103*, 3600.
(43) Dunning, T. H., Jr. *J. Chem. Phys.* **1989**, *90*, 1007.
(44) Kendall, R. A.; Dunning, T. H., Jr.; Harrison, R. J. *J. Chem. Phys.* **1992**, *96*, 6796.
(45) Lischka, H.; Shepard, R.; Pitzer, R. M.; Shavitt, I.; Dallos, M.; Muller, T.; Szalay, P. G.; Seth, M.; Kedziora, G. S.; Yabushita, S.; Zhang, Z. *Phys. Chem. Chem. Phys.* **2001**, *3*, 664.
(46) Köppel, H.; Cederbaum, L. S.; Domcke, W.; von Niessen, W. *Chem. Phys.* **1979**, *37*, 303.
(47) Mladenovic, M.; Schmatz, S.; Botschwina, P. *J. Chem. Phys.* **1994**, *101*, 5891.
(48) Sattelmayer, K.; Stanton, J. F. unpublished.